The American Journal of Pathology, Vol. 181, No. 1, July 2012

http://dx.doi.org/10.1016/j.ajpath.2012.03.030

Cell Injury, Repair, Aging, and Apoptosis

Retrograde and Wallerian Axonal Degeneration Occur Synchronously after Retinal Ganglion Cell Axotomy

Akiyasu Kanamori,* Maria-Magdalena Catrinescu,* Jonathan M. Belisle,*† Santiago Costantino,*† and Leonard A. Levin*‡

From the Maisonneuve-Rosemont Hospital Research Center and Department of Ophthalmology, and the Institute of Biomedical Engineering,† University of Montreal, Quebec, Canada; and the Department of Ophthalmology and Visual Sciences,‡ University of Wisconsin School of Medicine and Public Health, Madison, Wisconson*

Axonal injury and degeneration are pivotal pathological events in diseases of the nervous system. In the past decade, it has been recognized that the process of axonal degeneration is distinct from somal degeneration and that axoprotective strategies may be distinct from those that protect the soma. Preserving the cell body via neuroprotection cannot improve function if the axon is damaged, because the soma is still disconnected from its target. Therefore, understanding the mechanisms of axonal degeneration is critical for developing new therapeutic interventions for axonal disease treatment. We combined *in vivo* imaging with a multilaser confocal scanning laser ophthalmoscope and *in vivo* axotomy with a diode-pumped solid-state laser to assess the time course of Wallerian and retrograde degeneration of unmyelinated retinal ganglion cell axons in living rats for 4 weeks after intraretinal axotomy. Laser injury resulted in reproducible axon loss both distal and proximal to the site of injury. Longitudinal polarization-sensitive imaging of axons demonstrated that Wallerian and retrograde degeneration occurred synchronously. Neurofilament immunostaining of retinal whole-mounts confirmed axonal loss and demonstrated sparing of adjacent axons to the axotomy site. *In vivo* fluorescent imaging of axonal transport and photobleaching of labeled axons demonstrated that the laser axotomy model did not affect adjacent axon function. These results are consistent with a shared mechanism for Wallerian and retrograde degeneration. *(Am J Pathol 2012, 181:62–73; http://dx.doi.org/10.1016/j.ajpath.2012.03.030)*

Injury to mammalian central nervous system (CNS) axons causes their eventual dissolution, underlying the irreversible nature of disability from spinal cord injury, multiple sclerosis, glaucoma, and several other diseases.[1] Axonal degeneration after injury takes place both toward the proximal cell body (retrograde degeneration) and toward the distal axon terminal (Wallerian or orthograde degeneration). Although major advances have occurred in understanding cell death of the soma after axonal injury in the CNS, particularly with respect to Wallerian degeneration,[2] the understanding of axonal degeneration has lagged because there are relatively few methods for investigating axon loss in the nervous system during a span of time with sufficient spatial and temporal resolution. Conventional histological or ultrastructural methods using postmortem tissues provide an excellent static evaluation of axonal degeneration, but only at fixed times. Axonal degeneration has been quantitatively assessed for several days after injury in the spinal cord in the mouse,[3] the optic nerve in the rat,[4] and in the saphenous nerve using fibered fluorescence microscopy.[5] Real-time imaging of axonal degeneration in living animals (e.g., two-photon excitation microscopy of deeply located axons) is limited to a depth of 1 mm.[6] The methods used for these imaging procedures are invasive because the axons being studied are surgically exposed, with potential confounding by ischemic or traumatic effects on adjacent tissues.

The retina provides a unique platform for noninvasive imaging of CNS axons. Retinal ganglion cells (RGCs) are CNS neurons located within the innermost cellular layer of the retina. RGCs are output neurons for the retinal cells (photoreceptors, horizontal cells, bipolar cells, and ama-

Supported in part by grants from the Canadian Institutes for Health Research (MOP 84211), Canadian Foundation for Innovation, Canadian Research Chairs program, NIH (R21EY017970), and Research Fund in Ophthalmology of the University of Montreal.

Accepted for publication March 15, 2012.

Disclosures: L.A.L. serves as a consultant on neuroprotection for Allergan, Inotek, Merz, Quark, and Santhera.

Address reprint request to Leonard A. Levin, M.D., Ph.D., 5415 boul de l'Assomption, Montréal, Quebec H1T 2M4, Canada. E-mail: leonard.levin@umontreal.ca.

crine cells) that perform visual transduction and initial processing. Recent techniques in real-time imaging of axonal degeneration and axonal transport have provided valuable information on neurodegeneration.[3,5,7,8] Most of these techniques were first adapted for use on myelinated axons, which can differ from unmyelinated axons in the mechanism of degeneration.[9]

We and others have demonstrated that real-time confocal scanning laser ophthalmoscopy can be used to image RGC apoptosis,[10,11] intracellular signaling,[12] and intraretinal axonal degeneration[13] in rodents *in vivo*. Although the RGC response to transection within the optic nerve is well-defined histologically, with an initial dying back of the proximal segment within 24 hours, followed by regeneration to the cut end beginning by 2 weeks,[14] the longitudinal nature of the axonal response is less understood. Now we describe the noninvasive visualization of the dynamics of retrograde and Wallerian degeneration for up to 28 days after intraretinal axotomy of RGC axons. Unexpectedly, the rate and magnitude of retrograde and Wallerian degeneration in this model of transection of unmyelinated CNS axons were synchronous, suggesting a common mechanism for bidirectional axonal loss after injury within the CNS.

Materials and Methods

Intraretinal Axotomy

Animal experiments were approved by the Maisonneuve-Rosemont Hospital Research Centre Animal Care Committee and followed the Animal Care Guidelines of the Association for Research in Vision and Ophthalmology. Female Long-Evans rats weighing 225 to 250 g were obtained from Charles River (Saint-Charles, QC, Canada). All axotomy procedures were performed on the right eye under ketamine (50 mg/kg) and xylazine (100 mg/kg) anesthesia, with the left eye serving as a control. Pupils were dilated with phenylephrine and atropine. Animals with cataract or corneal problems that precluded imaging were not used further.

A commercially available confocal scanning laser ophthalmoscope (CSLO) (Heidelberg Retinal Angiogram 2; Heidelberg Engineering, Heidelberg, Germany) was modified by the addition of an animal laser injury platform based on a 200 mW 532 nm diode-pumped solid-state (DPSS) laser (Laserglow Technologies, Toronto, Canada) mounted on an optical breadboard (Thorlabs, Newton, NJ) with adjustable mirrors so that the DPSS laser output was aligned collinearly to the CSLO laser output (Figure 1A). Using a 30% transmission/70% reflection beam splitter, the 532 nm DPSS laser spot was localized on the retina while RGC axon bundles were visualized with the polarizing mode on the 488 nm CSLO laser (as follows). Low 532 nm laser power (approximately 0.1 mW) was used to target the beam to desired locations on the retina. Gross translations of the laser spot were achieved by changing the angle of the beam splitter in the horizontal and vertical planes or tilting of the head of the rat. Fine adjustments were achieved by a mirror mounted on a kinematic mount. The duration and power of the laser were varied under the control of a custom-written LabVIEW program (National Instrument, Austin, TX).

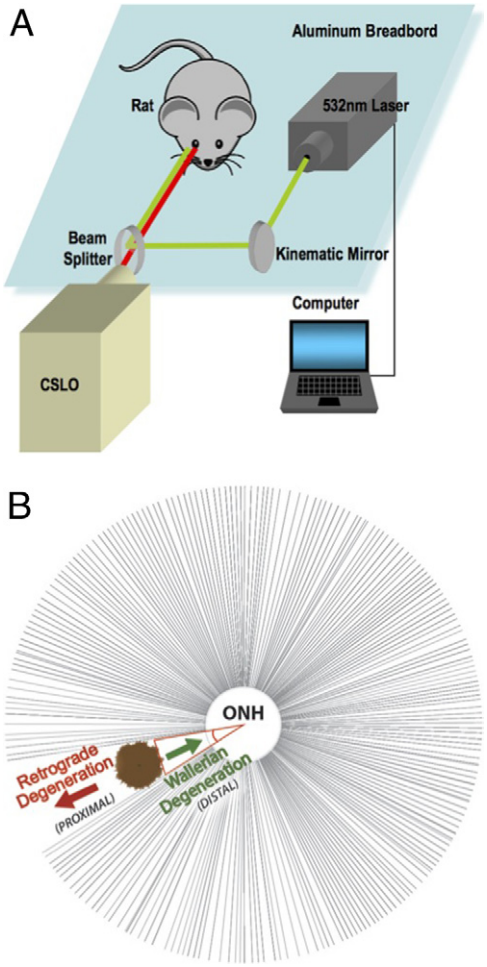

Figure 1. Schema of intraretinal laser axotomy. **A:** The 488 nm imaging beam of a CSLO was aligned collinearly with a 200 mW 532 nm diode-pumped solid-state laser using a kinematic mirror, and a 70/30 beam splitter. The 50 μm 532 nm laser spot was used for retinal photocoagulation at the same time that the retinal ganglion cell axon bundles were visualized with polarization-sensitive imaging by CSLO. **B:** The laser injury (irregular brown circle) causes retrograde degeneration toward the retinal ganglion cell bodies (not pictured) along the proximal axon and Wallerian degeneration along the distal axon and away from the cell body. The red triangle demarcates the degenerated axons, and the angle of its apex used to quantify the degree of axonal loss for *in vivo* and *ex vivo* comparisons. ONH, optic nerve head.

Fluorescent Labeling of Retinal Ganglion Cell Bodies and Axons

Fluorescent dyes 1,1′-dioctadecyl-3,3,3′,3′-tetramethylindotricarbocyanine iodide (DiR) (retrogradely transported infrared RGC label), MitoTracker Green FM (axonal mitochondria label), 5-chloromethylfluorescein diacetate (CMFDA) (axon label), and CellTracker Orange CMRA (axon label) were purchased from Invitrogen (Eugene, OR). The use of these dyes has the advantage of avoiding possibly neuronal toxicity from green fluorescent protein family probes.[15] Annexin B12 Cys101, Cys260- N, N′-dimethyl-N-(iodoacetyl)- N′-(7-nitrobenz-2-oxa-1,3-diazol-4-yl) ethylenediamine (annexin B12 Cys101, Cys260-IANBD)[16,17] was a kind gift from Ralf Langen,

University of Southern California. Intravitreal injections were performed as previously described.[12] Briefly, injections were made immediately posterior to the superotemporal limbus using a 32-gauge needle attached to a 10 μL Hamilton syringe (Hamilton, Reno, NV). Dyes (4 μL) were slowly injected through the sclera at a 45° angle. This route of administration avoided retinal detachment or injury to the lens or iris. Assuming the vitreous volume of an adult rat eye to be approximately 56 μL,[18] the final intravitreal concentrations of CMFDA, CMRA, and MitoTracker Green FM were approximately 60 μmol/L, 60 μmol/L, and 30 μmol/L, respectively. Erythromycin ophthalmic ointment was applied to the globe after injection. To avoid the possibility that the intravitreal injection process itself might cause transient retinal cellular injury, the counting of positive cells on CSLO was always performed at least 1 day after intravitreal injection of fluorescent dyes.

RGCs were retrogradely labeled by stereotactic injection of DiR into the superior colliculi. Briefly, the rats were placed in a stereotactic apparatus (Narishige Co. Ltd., Tokyo, Japan), and the skin of the skulls were incised. The brain surface was exposed by drilling the parietal bone to facilitate dye injection. DiR at a concentration of 20 mg/mL and 2.1 μL volume per side was injected bilaterally at 5.5 mm caudal to bregma and 1.2 mm lateral to the midline at a depth of 4.5 mm from the skull surface.

Confocal Scanning Laser Ophthalmoscopy

Three built-in CSLO lasers (488 nm, 788 nm, and 820 nm) were used for imaging. The 488 nm laser was used both in polarizing mode for imaging of retinal nerve fibers and in fluorescence mode for detection of MitoTracker Green FM, CMFDA, CMRA, and annexin B12 Cys101, Cys260-IANBD fluorescence emission from 500 to 650 nm. The excitation peaks for MitoTracker Green FM, CMFDA, CMRA, and annexin B12 Cys101, Cys260-IANBD are 490, 492, 548, and 525 nm, respectively. The excitation spectrum for the CMRA was broad enough to achieve an easily detected signal. The 788 nm laser was used for infrared fluorescence imaging of the retrograde labeling dye DiR, with detection of emission from 800 to 900 nm. The 820 nm laser was used for infrared reflectance imaging of the retinal pigment epithelium. Retinal imaging by CSLO was performed under ketamine/xylazine anesthesia. Pupils were dilated with phenylephrine and atropine. Retinal images were obtained using a 30° field of view and automatic real-time averaging of at least 50 images on the CSLO. To make a composite image, automatic real-time averaging composite mode was used.

Measurements of Laser Injury Size and Axonal Loss

Laser power and duration settings were systematically varied in preliminary experiments to optimize reproducible intraretinal axotomy with this model, while minimizing the lateral spread of thermal damage resulting from absorption by the retinal pigment epithelium. The diameter of the laser burn 1 day after injury was calculated by converting pixels (measured with the CSLO imaging analysis software) to micrometers based on the nominal length per pixel (1 pixel = 1.15 μm), as previously reported for the rat retina with a 30° field of view.[19] Two methods were used to measure the size of the laser burn: the diameter of the laser burn at the level of the retinal pigment epithelium, as imaged by infrared-reflectance; and the diameter of the laser burn at the level of the retinal nerve fiber layer, as observed by polarization-sensitive imaging. To assess axonal loss, polarization-sensitive images focused on the retinal nerve fiber layer were taken at 21 days after axotomy, by which time axon bundle loss could be clearly detected. The angle of the sector containing the degenerated fibers was calculated beginning from the optic nerve head (Figure 1B). These angular measures were correlated with subsequent neurofilament staining of axonal degeneration in the same retinas in whole-mounts.

To assess possible spread of RGC injury from the site of the laser burn through thermal conduction, apoptotic cells were detected by probing for externalization of phosphatidylserine with intravitreal annexin B12 Cys101, Cys260-IANBD[16,17] followed by CSLO.

Quantification of Retinal Ganglion Cell Somas

To quantify the reduction in RGC number after intraretinal axotomy, infrared CSLO images of DiR-labeled RGCs were longitudinally obtained in the retina peripheral to the laser burn (i.e., proximal to the axotomy site) before and 3, 7, 14, 21, and 28 days after axotomy. The same fields were selected at each imaging session. ImageJ (U.S. National Institutes of Health, Bethesda, MD) was used to process images for quantification. The images were rotated to orient the optic nerve head and the laser burn vertically. A 300 × 300 μm square field of retina 300 μm proximal to the proximal edge of the laser burn was captured. DiR-labeled RGCs within these fields were manually counted from randomized image files by an investigator masked to the experimental group. The number of labeled RGCs in the selected field after axotomy was compared to the number of labeled cells in the corresponding area before axotomy.

In Vivo *Imaging of Wallerian and Retrograde Axonal Degeneration*

To analyze the time course of Wallerian and retrograde axonal degeneration *in vivo*, 30° field of view images focused on the retinal nerve fiber layer were acquired proximal and distal to the laser burn using the 488-nm polarization-sensitive mode, before and 3, 7, 10, 14, and 21 days after axotomy. The same fields were selected at each imaging session. ImageJ (U.S. National Institutes of Health) was used to process images for quantification (Figure 2). The acquired images were rotated so as to orient the optic nerve head and the laser burn vertically. Square (512 × 512 pixel) fields (300 μm from the proximal and distal edges of the laser burn) were chosen. Each field was exported into a new window (Figure 2A). The rolling ball (radius at 50 pixel) transform was used to subtract background (Figure 2B). A fast Fourier transform was applied, the result convoluted with a filter designed to eliminate high spatial frequency horizontal structures (Figure 2C), and then inverted

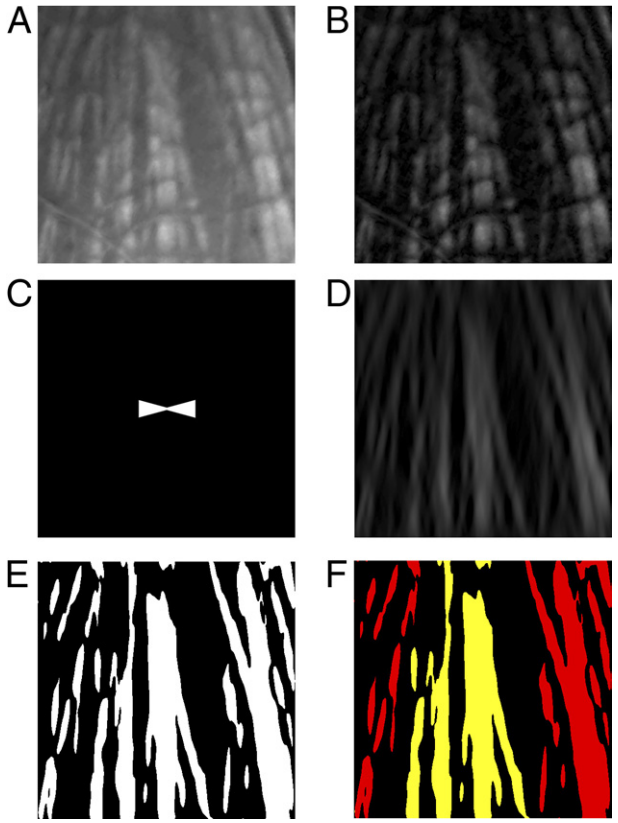

Figure 2. Image processing of the axonal degeneration with ImageJ (U.S. National Institutes of Health, Bethesda, MD). **A:** A square (512 × 512 pixel) polarization-sensitive image acquired by confocal scanning laser ophthalmoscopy was exported into a new window. **B:** A rolling ball subtraction (radius at 50 pixels) was used to subtract background. **C:** A fast Fourier transform (FFT) filter was created for eliminating small vessels from the analysis. **D:** An FFT image from (**B**) inverted through (**C**). **E:** The resultant image was segmented using Apply Threshold from Background, with the background chosen from an unaffected area near the axon, and then inverted to make axons white. **F:** The size of axons in the affected area (yellow) and the unaffected area (red) was calculated. The ratio of axons in the affected area to the unaffected area was 25%.

(Figure 2D). The inverted image was segmented using Apply Threshold from Background (scaling factor 5), with the background chosen from an area of retina near the axon bundles that did not itself contain axons. After the image was inverted to make axons appear white (Figure 2E), the area of bundles within the affected areas proximal and distal to the laser burn (Figure 2F) were calculated and normalized to the area of bundles in the adjacent uninjured retina. The axon survival rate was expressed as the ratio of the axon bundle area after axotomy to the area of bundles before axotomy.

Histology

Intact retinas for whole-mounts were removed immediately after euthanasia and fixed in 4% paraformaldehyde for 20 minutes at room temperature. The retinas were then blocked in 10% goat serum in PBS with 0.1% Triton X-100 for 2 hours, followed by incubation for 3 days at 4°C in mouse anti-neurofilament 200 kDa antibody (Sigma-Aldrich, St. Louis, MO) diluted 1:1000 and biotin-conjugated isolectin B4 (Sigma-Aldrich) at 5 μg/mL in blocking solution. After extensive washing in PBS with 0.3% Triton X-100, the retinas were incubated with Alexa Fluor 488-goat anti-mouse IgG (Invitrogen) at 10 μg/mL and AMCA-streptavidin (Jackson ImmunoResearch, West Grove, PA) diluted at 8 μg/mL for 24 hours in 4°C. Retinas were mounted on microscope slides with PermaFluor (Thermo Scientific, Waltham, MA) and observed by epifluorescence microscopy (Zeiss Axio Observer.A1; Carl Zeiss, Oberkochen, Germany).

Cryosections were used to assess the microstructural effects of laser burns in retinal sections. The cornea and lens were removed from enucleated eyes, and the eyecup was fixed for 30 minutes in 4% paraformaldehyde at room temperature. Following fixation, the eyes were cryopreserved with an increasing concentration of sucrose gradient and frozen in a 1:2 mixture of Tissue-Tek OCT (Sakura Finetek, Torrance, CA) and 20% sucrose. Retinal cryosections (8 μm) in the sagittal plane were stained with H&E.

Statistics

Results are presented as mean ± SEM. Unpaired *t*-tests were used for comparisons between two groups. The Spearman rank correlation coefficient was used for the calculation of relationship. $P < 0.05$ was considered statistically significant.

Results

In Vivo *Imaging of Burn Size at Different Laser Durations and Power*

Single areas of rat retinas were focally coagulated with a transpupillary DPSS 532 nm laser (National Instrument) and simultaneously visualized by polarization-sensitive and fluorescence imaging by CSLO through a 70/30 beam splitter, using coaxially aligned laser beams. This *in vivo* imaging allowed fine adjustment of the laser spot concurrent with viewing of axonal bundles. Two or three lesions were created approximately 800 μm from the optic nerve head. Thirty eyes were used for these analyses, which were all studied 1 day after axotomy. The diameter of the laser burn measured 24 hours later by *in vivo* infrared-reflectance (Figure 3A) imaging, which detects injury at the level of the retinal pigment epithelium, or by polarization-sensitive (Figure 3B) imaging, which detects disruption of axonal microtubules (either from edema or transection), strongly correlated with the laser duration (Figure 3C) and power (Figure 3, D and E). The diameter of the laser burns gradually decreased in time, presumably from contraction.

In Vivo *Imaging of Axonal Loss at Different Laser Injury Energies*

Pilot experiments using polarization-sensitive imaging revealed axonal loss starting 7 days after intraretinal axotomy with the 532 nm DPSS laser at 50 μm beam size. To refine the conditions, durations from 1 to 27 seconds were tested at 70 and 140 mW laser power with the goal of achieving reproducible axonal loss, as measured *in vivo* and in retinal whole-mounts. The latter were neces-

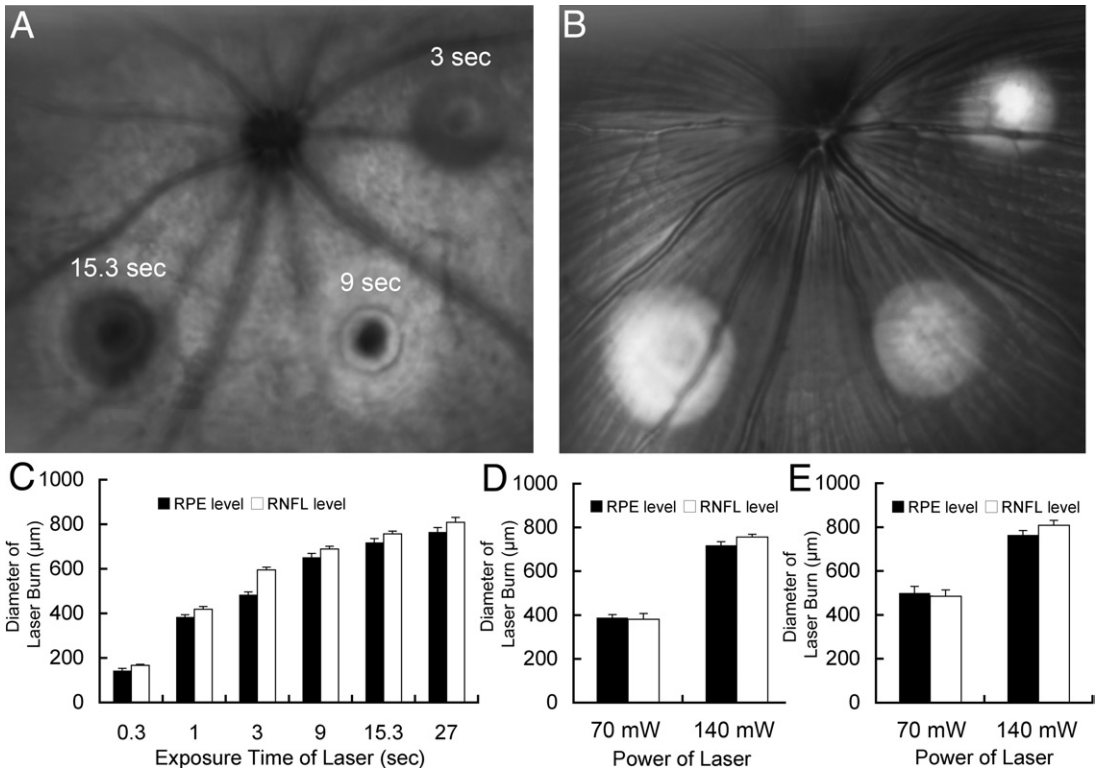

Figure 3. Size of laser burns with different laser exposures. The diameters of the laser burns 1 day after injury were correlated with the exposure time and power of the laser. **A**, **B:** A composite image using infrared reflectance imaging by confocal scanning laser ophthalmoscopy at the RPE level (**A**) and polarization-sensitive imaging at the RNFL level (**B**). The power of the laser was held constant at the maximum available (140 mW), and the duration of the burn varied. **C:** Diameters of the imaging changes in the RPE and the RNFLs were measured at different laser durations (n = 6 to 24), with the power of the laser held constant at 140 mW. **D**, **E:** Diameters of affected RPE and RNFL with durations of 15.3 seconds (sec) (**D**) and 27 sec (**E**) were compared at powers of 70 mW (n = 3) and 140 mW (n = 6 to 11).

sary to confirm that the polarization-sensitive imaging changes reflected axon loss and not just edema. The angle of the sector containing the degenerated axons was calculated from polarization-sensitive *in vivo* imaging by CSLO, followed by staining for neurofilaments of the same retinas in whole-mounts (Figure 4, A and B). The axonal loss on polarization-sensitive *in vivo* imaging was evaluated with different laser settings in 30 eyes (Figure 4, C and D). A dose-dependent effect of laser duration on axonal loss measured by CSLO was observed when the power was 140 mW. No detectable axonal loss occurred with 0.3-second duration. Laser durations of 1 and 3 seconds induced minimal axonal loss, but 9 seconds or more caused significant axonal loss. There were no significant differences in axonal loss among 9, 15.3, and 27 seconds duration at 140 mW power. In comparison, 15.3 or 27 seconds duration at 70 mW laser power did not induce detectable axonal loss (data not shown). Based on these preliminary data, we chose a laser burn of 15.3 seconds at 140 mW for subsequent studies of intraretinal axotomy to minimize secondary effects of laser injury. The angle of the sector calculation (Figure 4, A and B) was done in 13 retinas that received a total of 25 laser burns. As expected, axonal loss measured by *in vivo* imaging and histological examination were significantly correlated (r = 0.92; $P < 0.0001$; n = 25) (Figure 4D).

Histological Identification of Axonal Loss after Focal Laser Injury

Immunostaining of retinal whole-mounts for neurofilaments visualized the trajectory of axons (Figure 5A). Isolectin B4 was used to identify blood vessels, which allowed the alignment of the *ex vivo* retinal whole-mounts (Figure 5A) with the *in vivo* polarization-sensitive images (Figure 5B). A 9-second laser burn at 140 mW induced histologically evident axonal loss, but not a 1-second burn. The morphology and degree of axonal loss in retinal whole-mounts was highly concordant with that seen on CSLO imaging. All retinal layers were affected by a 15.3-second laser burn (Figure 5C). Areas more than 300 microns from the center of the laser burn maintained normal retinal architecture (Figure 5D). Apoptotic cells (detected by probing with annexin B12 Cys101, Cys260-IANBD 7 days after injury) could be observed only at the site of the laser burn and at various locations along the course of the injured axons (Figure 5, E and F).

Quantification of Retinal Ganglion Cells in Vivo *after Intraretinal Axotomy*

Axotomy causes the death of mammalian central neurons. To assess RGC soma loss after intraretinal axotomy, RGCs were retrogradely labeled with the infrared fluores-

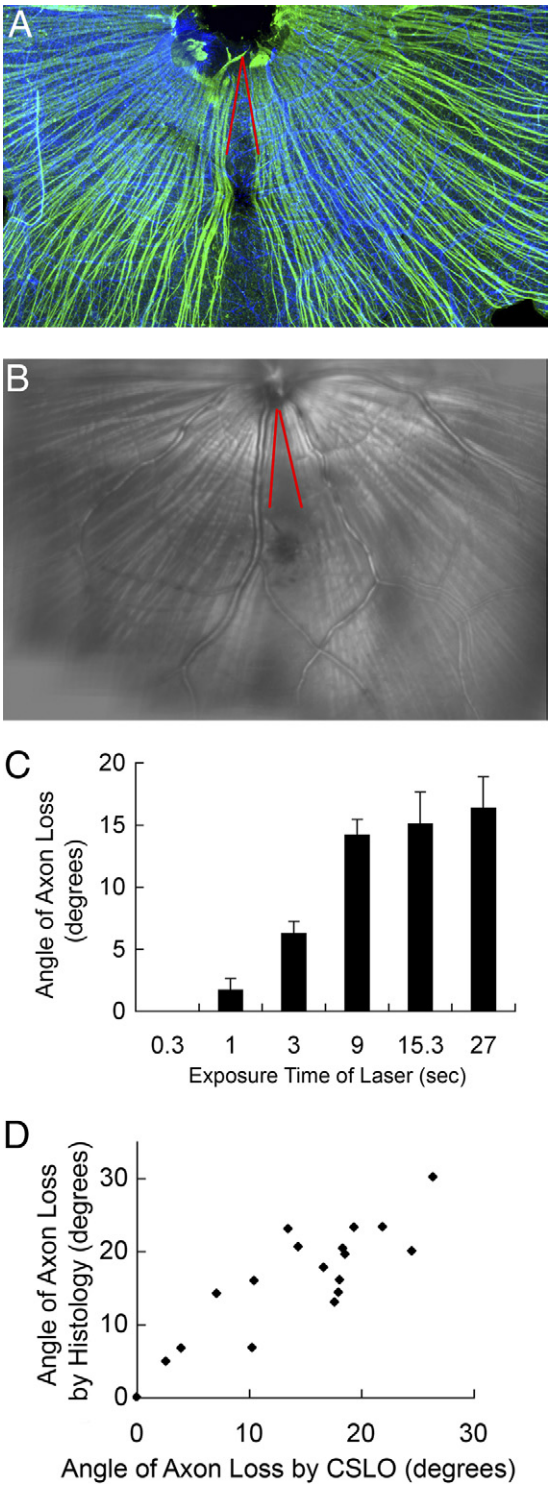

Figure 4. Axonal loss after intraretinal axotomy at different durations of laser delivery. **A**, **B:** Angle of sector (red) consisting of degenerated axons in (**A**) retinal whole-mounts and (**B**) polarization-sensitive imaging by CSLO were measured from the optic nerve head. **A:** Retinal whole-mounts were immunostained for axons with anti-neurofilament 200 kD antibody (green) and for blood vessels with isolectin B4 (blue). Composite image (**B**) on polarization-sensitive imaging on CSLO corresponding to **A**. **C:** The angle of degenerated axons at a different duration of laser (n = 6 to 24). The angle was measured on polarization-sensitive imaging by CSLO at 21 days after intraretinal axotomy by laser (140 mW). **D:** Scatter plot of angles of degenerated axons from retinal whole-mounts and polarization-sensitive imaging on CSLO, which were highly correlated (r = 0.92; $P < 0.0001$; n = 25). sec, seconds.

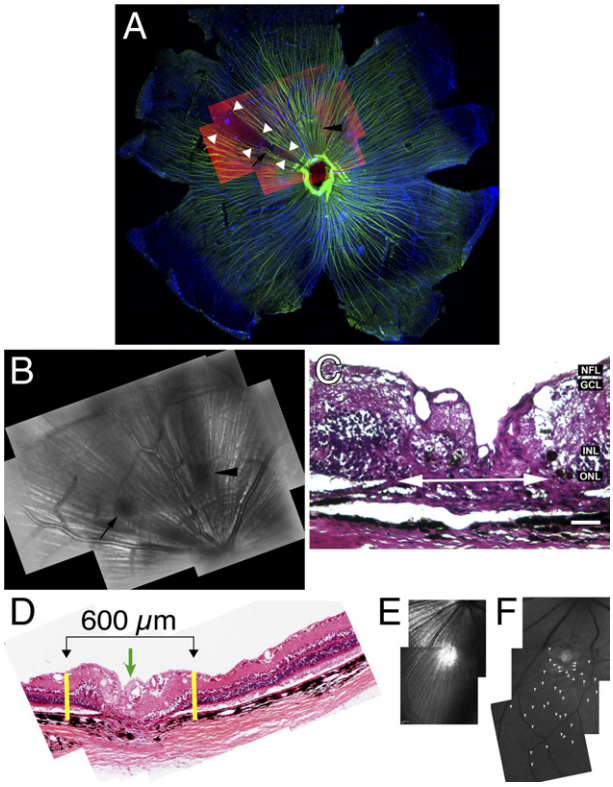

Figure 5. Histological examination of intraretinal axotomy. **A**, **B:** Axonal loss on confocal scanning laser ophthalmoscopy was confirmed on retinal whole-mounts at 21 days after axotomy. **Black arrow** and **black arrowhead** indicate lesions induced by 9- and 1-second laser burns. **A:** A retinal whole mount was immunostained for neurofilaments (green) and isolectin B4 (blue). **Red inset** shows the same field as in **B**, aligned using vessels as landmarks. **White arrowheads** indicate the loss of axons. **B:** A composite image on polarization-sensitive imaging just before immunostaining corresponding to **A**. **Black arrow** and **black arrowhead** indicate lesions induced by 9- and 1-second laser burns. **C:** A retinal cross-section stained with H&E shows laser bundle loss at 21 days after a 15.3-second laser burn. **White arrow** indicates laser bundle damage. All neuronal retinal layers at the site of the laser burn lesion were damaged, but the ganglion cell and retinal nerve fiber layers were additionally lost away from the laser burn. GCL: ganglion cell layer; INL: inner nuclear layer; NFL, nerve fiber layer; ONL: outer nuclear layer. Scale bar = 100 μm. **D:** Collage of retinal cross-sections demonstrating preservation of retinal layers away from the center of a 9-second laser burn (**green arrow**). The distance between the yellow lines delimiting the abnormal retina/retinal pigment epithelium (RPE) is 600 μm. **E:** Polarization-sensitive in vivo imaging 7 days after laser burn. **F:** Corresponding fluorescence image after intravitreal injection of annexin B12 Cys101, Cys260-IANBD, detecting apoptotic retinal ganglion cell (RGC) somas. **White arrowheads** mark RGC somas distributed in a pattern corresponding to the axons affected by the burn.

cent dye DiR injected into the superior colliculi and then visualized *in vivo* using the 788 nm laser on the CSLO. Axotomy was performed at 10 sites in 6 retinas of 6 rats with 140 mW laser power for a 15.3-second duration. Reduction of RGC numbers was longitudinally observed starting from before axotomy to 28 days after axotomy. Visualization of the same retinal area was achieved by using the retinal vessels as fiduciary marks between imaging sessions. Both affected RGCs (those projecting axons through the injury site) and unaffected RGCs (those projecting axons away from the injury site) were counted. A wedge-shaped area of RGC loss could be identified peripheral to the laser burn starting 21 days after axotomy (Figure 6, A and B), with most of the loss occurring between 3 and 7 days and then continuing at a

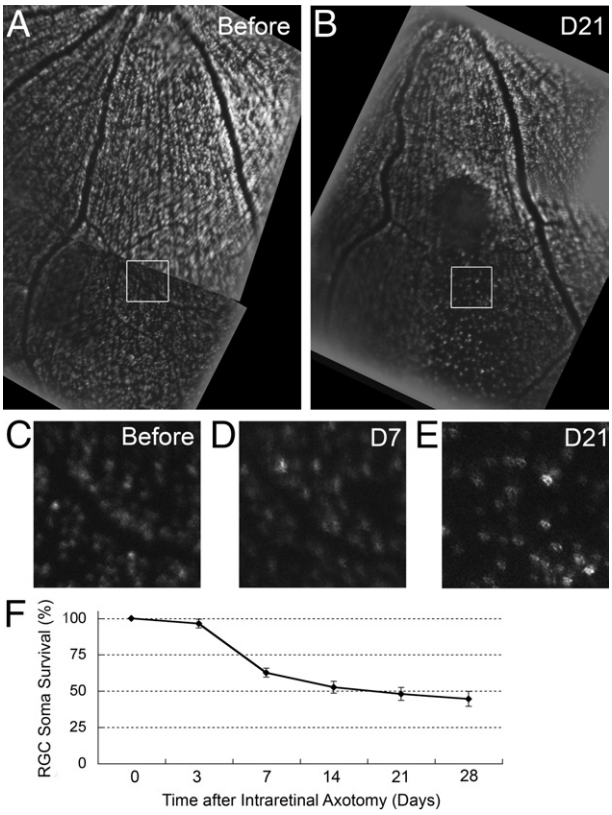

Figure 6. Loss of retrograde-labeled retinal ganglion cells (RGCs) after intraretinal axotomy. **A**, **B:** Composite image of 1,1′-diocta-decyl-3,3,3′,3′-tetramethyl-indo-tri-carbo-cyanine iodide (DiR)-positive RGCs detected by confocal scanning laser ophthalmoscopy before (**A**) and 21 days (D21) after (**B**) intraretinal axotomy. RGCs were previously retrogradely labeled by injection of DiR into the superior colliculi. RGCs were counted within a 300 μm × 300 μm square (**inset**) located 300 μm away from the edge of the laser burn. **C–E:** Series of image captures of DiR-labeled RGCs in the area corresponding to the **inset** in (**B**) before (**C**) and at 7 days (D7) (**D**), and 21 days (**E**) after intraretinal axotomy. The darkened square area is an artifact of imaging, and does not reflect a lower number of DiR-labeled RGCs in that area. **F:** Survival of RGCs after intraretinal axotomy was longitudinally evaluated as a percentage of the number visible in the same retinal area at baseline before axotomy (n = 10).

lower rate through 21 days after axotomy (Figure 6, C–F). There was no loss of RGCs that did not project axons through the site of axotomy. In particular, there was no loss of RGCs adjacent to the site of axotomy (ie, there was no secondary degeneration of laser-injured RGC somas up to 28 days after injury).

Quantification of Retrograde and Wallerian Degeneration in Vivo *after Intraretinal Axotomy*

Axonal degeneration proximal and distal to the site of the laser burn was longitudinally evaluated from before axotomy to 21 days after axotomy by polarization-sensitive imaging with the CSLO. The same parameters for laser injury, a 15.3-second duration and 140 mW, were used as with imaging RGC soma death. There were 10 laser burns performed in 6 retinas of 6 rats, 3 of which were also imaged for assessing RGC soma death (see previously). The selected fields proximal and distal to the axotomy site (Figure 7A) were chosen so as to contain both affected axons (projecting through the injury site) and unaffected axons (not projecting through the injury site). Axonal degeneration could be qualitatively identified on polarization-sensitive imaging as a decrease in the intensity and size of parallel axon bundles (Figure 7, B, D, and F). To objectively quantify the reduction of axons, image processing was performed with ImageJ (U.S. National Institutes of Health). Frequency domain filtering after two-dimensional Fourier transformation was used to eliminate nonaxonal structures, such as small vessels running orthogonal to the axons (Figure 7, C and E). Large vessels running parallel to axon bundles could not be eliminated by this filtering procedure, and therefore areas for analysis were chosen that did not contain such vessels.

The area of intact axons proximal to the injury site decreased steadily from 7 to 21 days after axotomy (Figure 7G, red line). Only 8% of axons that were visible before axotomy were present at 21 days after axotomy. The area of axons distal to the injury site, as a proportion of those visible before axotomy, decreased at a similar rate to those proximal to the injury site, with 9% visible at 21 days (Figure 7G, blue line). There were no significant differences between proximal and distal axonal loss at each time point after axotomy. There was no spread of loss of RGC axons (ie, there was no secondary degeneration of laser-injured RGC axons up to 21 days after injury).

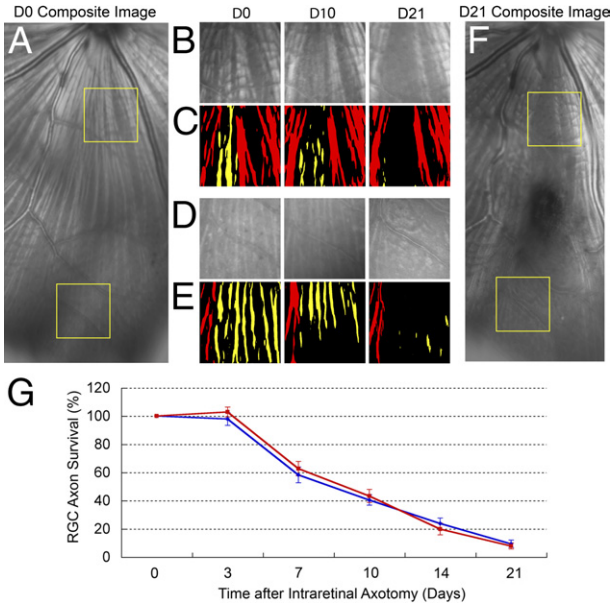

Figure 7. Axonal degeneration with a duration of time after intraretinal axotomy. **A:** A composite image before intraretinal axotomy from a representative case. **Yellow squares** indicate the selected fields that were used in quantitative analyses. **B–E:** Series showing retrograde (**D** and **E**) and Wallerian (**B** and **C**) degeneration from the polarization-sensitive images (**B** and **D**) and the processed images (**C** and **E**). **F:** A composite image at 21 days (D21) after intraretinal axotomy. **G:** The survival ratios of proximal (red) and distal (blue) axons were calculated as the ratio of affected axons to unaffected axons. The ratio before axotomy was set at 100%. The time course and magnitude of retrograde and Wallerian degeneration was nearly identical. D0, 0 days; D10, 10 days; RGC, retinal ganglion cell.

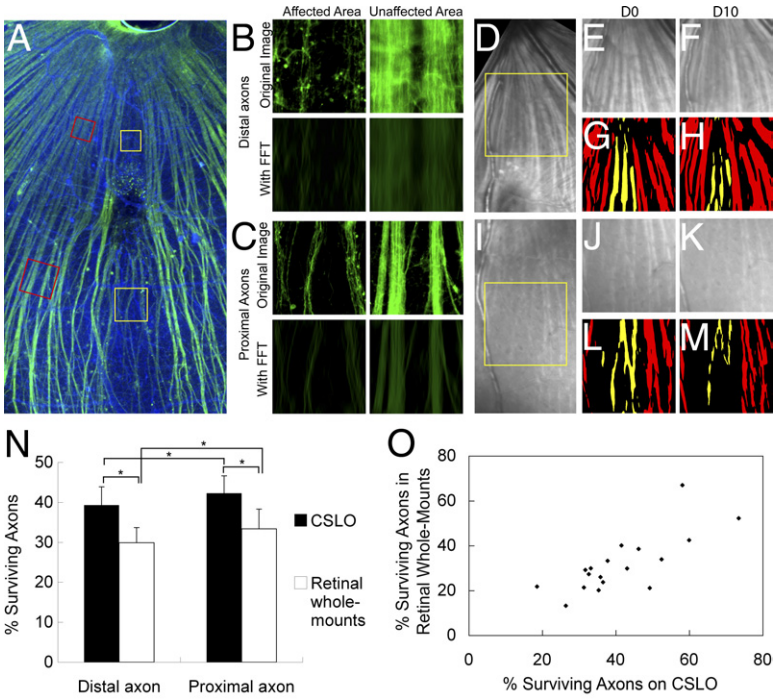

Figure 8. Correlation of axonal degeneration measured by polarization-sensitive imaging with retinal whole-mounts. **A:** Retinal whole-mounts from 10 days after intraretinal axotomy were stained for neurofilament 200 kDa (green) and isolectin B4 (blue). **B, C:** Distal (**B**) and proximal (**C**) axons in the affected (**left**) and the unaffected (**right**) area from retinal whole-mounts stained for neurofilaments. The images of the affected and unaffected areas correspond to the **yellow squares** and **red squares** in **A**, respectively. **Bottom** shows the images after a fast Fourier transform (FFT) was performed on the original images (**top**). The survival ratios on distal and proximal axons were 27% and 31%, respectively. **D**, **I:** Polarization-sensitive imaging on confocal scanning laser ophthalmoscopy (CSLO) using a 30° field of view of distal (**D**) and proximal (**I**) axons was acquired just before the extraction of retina in **A**. **Yellow squares** show the quantitative areas as shown in **E–M**. **E, F:** Polarization-sensitive images of the distal axons before (**E**), and at 10 days after (**F**) intraretinal axotomy. **G**, **H:** Image processing was performed as in **E** and **F**. The survival ratio of axons was 34%. **J, K:** Polarization-sensitive images of the proximal axons before (**J**) and at 10 days after (**K**) intraretinal axotomy. **L, M:** Image processing was performed as in **J** and **K**. The survival ratio of axons was 33%. **N:** There were no significant differences between the survival of the proximal and distal axons either on polarization-sensitive imaging *in vivo* or after staining for neurofilament 200 kDa in retinal whole-mounts. *Not significant. **O:** Scatter-plot of survival based on polarization-sensitive imaging versus neurofilament staining in retinal whole-mounts ($r = 0.76$; $n = 18$; $P < 0.001$).

Histological Quantification of Axonal Degeneration Proximal and Distal to Intraretinal Axotomy

To correlate the loss of axons by polarization-sensitive imaging with histological disappearance of axons, axonal degeneration on both sides of the axotomy site was assessed in retinal whole-mounts. Immediately after the 10-day postaxotomy imaging session, 5 rats were euthanized and 5 retinas containing 9 axotomized areas were immunostained for neurofilaments (Figure 8, A–C). Intraretinal axotomy was at 140 mW for either 9 seconds ($n = 4$) or 15.3 seconds ($n = 5$). To quantitate the axonal survival ratio, retinas were initially assessed with a 2.5× objective lens on an epifluorescence microscope to determine the approximate area of involved retina. Images of proximal and distal axons were then digitally captured with a 20× objective lens at the same exposure setting and rotated to maintain orientation across imaging sessions. A 512 × 512 pixel square field containing only axotomized axons was selected proximal to the axotomy site and a 256 × 256 pixel field selected distal to the axotomy site. A smaller field was chosen for the distal axons because a 512 × 512 pixel field would be larger than the area of axons and therefore also contain untransected axons (Figure 8A, yellow inset). Identically sized control fields containing only untransected axons were selected lateral to both sites of axotomy and at the same radial distance from the optic nerve head (Figure 8A, red inset). Axotomized axons were compared to untransected axons in control fields because histological studies could not be done longitudinally in the same animal. Immunostaining for neurofilaments identified not only RGC axons, but also somas and dendrites (Figure 8, B and C top). After two-dimensional filtering in the frequency domain using the same filter as used for the CSLO image analysis (Figure 2C), most fluorescence of RGC somas and dendrites could be eliminated (Figure 8, B and C, bottom). Axonal degeneration measured by polarization-sensitive CSLO *in vivo* (Figure 8, D–M) was compared to histological examination of retinas from animals euthanized immediately after imaging.

The number of histologically evident axons proximal and distal to the axotomy site at 10 days was approximately one third of that in the control (unaffected) areas of the retina, which did not contain axotomized axons (Figure 8N, white bars). There was no significant difference between the number of proximal and distal axons surviving after intraretinal axotomy (33.4 ± 4.9% versus 29.9 ± 3.8%; $P = 0.32$), as measured in retinal whole-mounts. The proportion of CSLO visible axons proximal and distal to the axotomy site at 10 days after laser burn decreased to 42.3 ± 4.4% and 39.3 ± 4.6% of the number before axotomy, respectively ($n = 9$) (Figure 8N black bars). There was no significant difference in the proportion surviving between proximal and distal axons measured *in vivo* imaging ($P = 0.29$). The proportion of surviving proximal (42.3 ± 4.4% versus 33.4 ± 4.9%; $P = 0.097$) and distal (39.3 ± 4.6% versus 29.9 ± 3.8%; $P = 0.067$) axons measured by CSLO was somewhat more than that measured histologically. To better understand the relationship of axonal imaging between polarization-sensitive imaging of RGC axons *in vivo* and histological examination of neurofilament-stained retinal whole-mounts *ex vivo*, the number of axons in identical fields was compared between both methods. The number of surviving axons by *in vivo* imaging significantly correlated with that determined by immunostaining for neurofilament ($r = 0.76$; $P <$

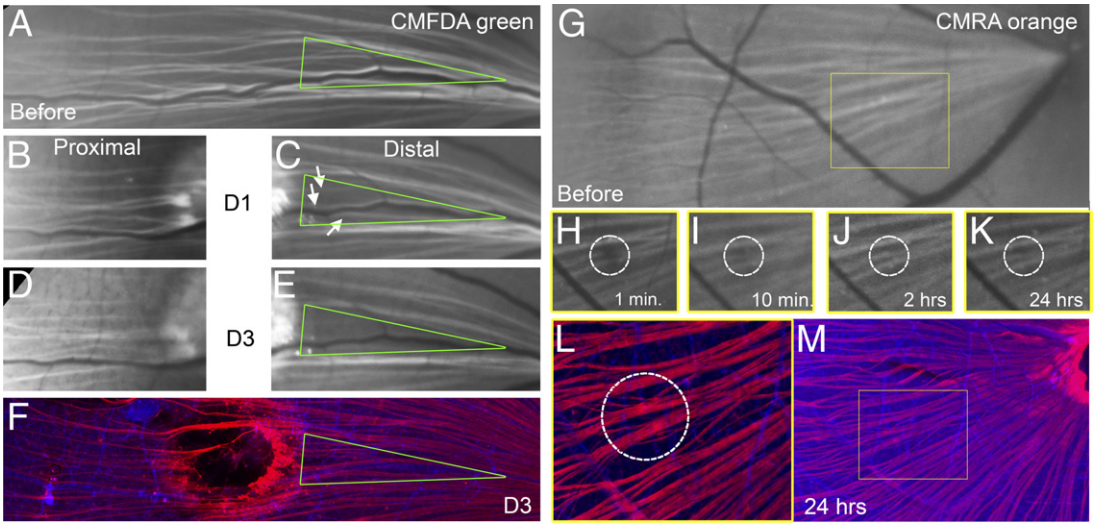

Figure 9. Real-time imaging of axons by 5- CMFDA (**A–F**) and CMRA (**G–M**). RGC axons were visualized by intravitreal injection of CMFDA and CMRA. Distal axons lost CMFDA staining within 3 days after axotomy (**green triangle**) (**C** and **E**). In contrast, proximal axons retained CMFDA staining (**B** and **D**). Neurofilament staining (red) in whole mount retina revealed intact RGC axons outside the laser burn (**F**). A 1-minute (min) exposure to a diode-pumped solid-state laser (532 μm) at 1 mW bleached CMRA staining (**H, circle**). The bleached lesion began recovering fluorescence within 10 minutes after bleaching (**I**), and returned to the pre-bleaching condition at 2 hours after bleaching (**J**). After imaging at 24 hours after laser (**K**), the retina was removed and rapidly stained for neurofilaments (**L,** high magnification; **M**, low magnification). Bleaching did not cause morphological damage to axons. **Yellow squares** indicate the same field on *in vivo* imaging and on a retinal whole-mount.

0.001; $n = 18$) (Figure 8O). The slope was 0.73 ± 0.16, suggesting that the image analysis by CSLO somewhat underestimated axonal degeneration compared to histological examination.

Real-Time Visualization of Axonal Transport by in Vivo *Imaging*

One explanation for the previous findings of synchronous retrograde and Wallerian degeneration after laser axotomy was that this was a result of diffusion of thermal damage on axonal transport outside the treated area. To address this, the thiol-reactive fluorescent dye CMFDA was injected intravitreally, labeling a single patch of RGC somas and their distal axons.[13] Intense labeling of RGC axonal bundles by CMFDA could be visualized using the 488 nm laser on the CSLO (Figure 9A). After laser axotomy, axon segments distal to the injury site lost CMFDA fluorescence within 3 days (Figure 9, B–E). In contrast, axon segments proximal to the injury site remained fluorescent. Histological examination revealed that both distal and proximal axon segments remained morphologically intact at 3 days after axotomy (Figure 9F). This pattern is consistent with interruption of anterograde axonal transport of CMFDA only at the site of laser damage, and not away from the injury. There was no requirement for microtubules in the early transport of CMFDA, based on a failure of intravitreal calpain (100 μmol/L) and ethyl(+)-(2S,3S)−3-[(S)−3-methyl-1-(3-methylbutyl-carbamoyl)butyl-carbamoyl]-−2-oxi-rane-carboxylate (EST) (100 μmol/L) to affect the CMFDA-staining pattern after axotomy (data not shown). There was little evidence for abortive RGC regeneration, which is usually seen after 2 to 4 weeks,[14,20,21] and would be minimal at 3 days.

To confirm that CMFDA assayed axonal transport, we also used CMRA, which is chemically highly similar to CMFDA but excites at a longer wavelength, and thus is amenable to photic bleaching without axonal damage. After labeling of RGC axons with CMRA (Figure 9G), the 532 nm DPSS laser was used to bleach a small spot of CMRA-labeled axons and longitudinally followed. Immediately after laser exposure, the bleached lesion was detected as a hypofluorescent area (Figure 9, H–K). Fluorescence began reconstituting from the edges within 10 minutes and completely recovered at 2 hours after bleaching. During this period, the bleached area did not move in either direction along the axon. Neurofilament-stained retinal whole-mounts revealed no morphological changes associated with laser bleaching (Figure 9, L and M). These results are consistent with bidirectional transport of CMRA.[22]

Finally, the interruption of axonal transport of mitochondria by laser axotomy was examined. MitoTracker Green FM passively diffuses across the plasma membrane and accumulates in respiring mitochondria, and is transported from RGCs or axon segments located at the injection site. Intravitreal injection of MitoTracker Green FM resulted in a similar pattern of RGC axonal fluorescence to that seen with CMFDA (Figure 10A). By 1 day after axotomy, proximal axons had increased fluorescence of MitoTracker Green FM at the edge of the laser burn (Figure 10B), and at 3 days the proximal axons were even brighter (Figure 10D). In contrast, distal axons started losing MitoTracker Green FM fluorescence at 1 day after axotomy (Figure 10C), and at 3 days there was only faint fluorescence remaining (Figure 10E). As with CMFDA, the axons proximal and distal to the burn were morphologically intact at the same time (1 and 3 days) that axonal transport was interrupted. This pattern is virtually identical to that seen with CMFDA. Together these results support an interruption of transport at the injury site but not proximal or distal to it.

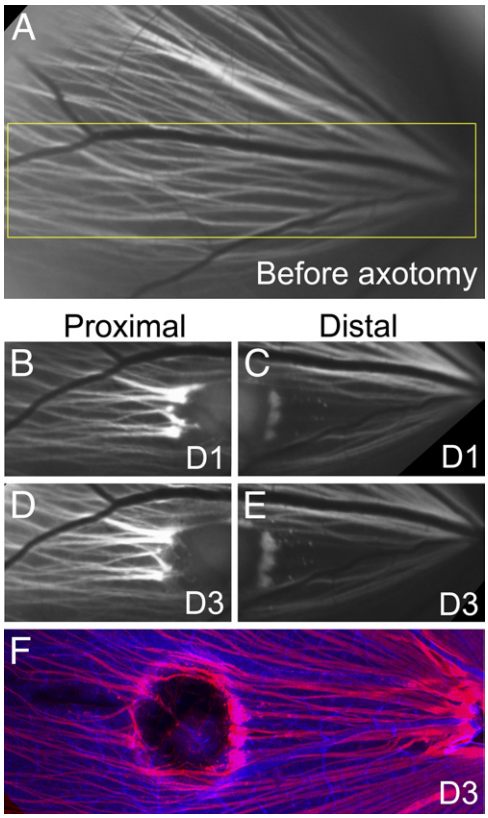

Figure 10. Real-time imaging of axons with MitoTracker Green FM. **A:** A composite image of RGC axons visualized by intravitreal injection of MitoTracker Green FM. **Yellow square** indicates the same field as **B–F**. Axons proximal to the laser burn demonstrated stronger MitoTracker Green FM fluorescence at 1 day (**B**) and 3 days (**D**) after axotomy. In contrast, staining in the axons distal to the injury decreased at 1 day (**C**) and stabilized at 3 days after axotomy (**E**). **F:** Retinal whole-mounts removed from the eye at 3 days after laser axotomy demonstrated that these axons were morphologically intact (red, neurofilaments; blue, blood vessels).

Discussion

Axonal degeneration has been recognized as a critical element in the pathophysiology of several neurological diseases,[23] and underlies almost all optic neuropathies.[24] We took advantage of the clarity of the ocular media to directly and noninvasively image degeneration of axons coursing within the nerve fiber layer of the superficial retina for several weeks. Unexpectedly, we found that the retrograde and Wallerian degeneration of these unmyelinated RGC axons occurred with a nearly identical time course and to a similar magnitude. To our knowledge, this is the first study to noninvasively examine longitudinal CNS axonal degeneration on both sides of an injury by *in vivo* imaging.

The study of axonal degeneration *in vivo* is highly dependent on imaging techniques, which in most cases requires exposure of overlying tissue. Others have observed axonal degeneration *in vivo* in tissues that necessitated incisional surgery,[3–5] and confocal scanning laser ophthalmoscopy has been previously used to evaluate retrograde (but not Wallerian) degeneration from RGCs after optic nerve transection or crush.[13,25] These differences in technique may explain why the finding of synchronous retrograde and Wallerian degeneration may not have been previously detected. The evaluation of axonal degeneration on polarization-sensitive imaging *in vivo* also necessitates specialized image processing, unlike quantification of intensity of a fluorescent dye that stained axons.[13] To eliminate other retinal structures and avoid subjective bias, image processing was done with ImageJ (U.S. National Institutes of Health) (Figure 1). Immunostaining for neurofilaments supported the quantification of axonal degeneration by real-time CSLO. As expected, RGC cell loss accompanied axonal loss.

Several experiments were performed to confirm that the laser axotomy model did not have artifactual effects on axon structure or function. We used a DPSS continuous wave laser for axotomy, which causes damage to the other retinal layers in the area of the focused laser beam. A femtosecond laser could not be used because the numerical aperture of the rat eye is too low to allow sufficient power delivery to the retinal nerve fiber layer alone without injury to the adjacent retinal layers. Because of the possibility for confounding from injury to other retinal layers, we only analyzed axons outside the area of the laser burn. Intraretinal axotomy did not cause significant thermal or mechanical damage outside the laser burn, nor did the loss of inner and outer nuclear layer cells in the retina cause indirect axonal damage, based on the fact that the loss of retrograde-labeled RGCs was only observed in retinal locations proximal to the site of axotomy and that histological examination of the retina more than 300 μm away from the burn was normal. Furthermore, apoptotic RGCs (detected *in vivo*) were only present at the site of the laser burn and in the expected nerve fiber bundle pattern corresponding to the distribution of the injured axons. This observed distribution makes spread of thermal injury, which would result in a large circle of apoptotic cells, an improbable cause of the observed radial pattern of axonal injury. If the laser burn area to the adjacent RGC axons caused spreading of injury, then the axon bundle would be wider than that of the burn, contrary to what was observed. Similarly, a release of factors from dying retinal neurons or glia in other layers of the retina is unlikely because the locus of axonal loss with a duration of time followed the nerve fiber bundle distribution that was observed with all three methods: i) *in vivo* CMFDA labeling, ii) *in vivo* polarization-sensitive imaging, and iii) *ex vivo* neurofilament staining of axon visualization.

These controls, therefore, ruled out artifactual effects of laser injury on axonal structure. Then we tested whether spread of thermal injury from the laser affected axonal function, specifically, anterograde axonal transport. To do this, we studied axonally transported CMFDA, MitoTracker Green FM-labeled mitochondria, and CMRA photobleaching. Once inside cells, CMFDA and CMRA are hydrolyzed to a polar and relatively cell-impermeant fluorescent thioether adduct. Although the exact mechanism of CMFDA and CMRA staining in axons is unclear, CMFDA and CMRA have similar chemistries, and based on their pattern of fluorescence over time, they can be used to grossly assess axonal transport. MitoTracker Green FM directly labels mitochondria, which themselves undergo axonal transport. With all three

dyes, there was no effect on axonal transport other than the expected blockade at the laser burn itself. This supports a focal effect of the laser injury on axonal function.

There are several situations in which there is a symmetry of the response of the proximal and distal axon to axotomy. *In vitro* models usually show a similar rate of degeneration.[26] The earliest axonal response to transection is a calcium wave-dependent calpain activation and depolymerization of microtubules immediately adjacent to the injury site, followed by disorganization of the axonal plasmalemma.[27–29] These responses are symmetric.[30] The surviving distal axon can continue both anterograde and retrograde axonal transport.[31] In invertebrates, the proximal and distal ends of the axon can survive transection for extended periods.[32,33] Also, when there is an immediate regeneration potential, as in the peripheral nervous system, a growth cone initiates on both the proximal and distal ends, but it withers on the distal end.[34]

Conversely, there are differences between what happens to the proximal versus distal axons after axotomy. Retrograde and Wallerian degeneration share features of axonal dissolution, but necessarily differ because retrograde degeneration involves the proximal segment, which is by definition contiguous with the cell soma, whereas Wallerian degeneration involves the distal (isolated) segment. Wallerian degeneration, therefore, is a consequence of the separation of the distal axon from its metabolic support from the cell body; retrograde degeneration in the proximal axon is a consequence of the proximal axon being deprived of growth factors from the postsynaptic target. This distinction has implications for systems in which regeneration is the norm (eg, the peripheral nervous system), with consequent asymmetric development of the neuronal growth cone at the cut ends,[34] as well as the mammalian CNS, in which the regeneration is abortive but incomplete.[35,36] Proximal axons remain stable for a longer period than distal axons.[37] Kerschensteiner et al [3] observed axonal degeneration of sensory neurons in dorsal root ganglions in real-time using transgenic Thy-1-green fluorescent protein mice. Identical degeneration at both the proximal and distal ends was observed as early as 30 minutes after injury. They named this early event of simultaneous degeneration "acute axonal degeneration," which proceeded at both sites within 4 hours after injury. However, after approximately 30 hours, only the distal axons began to rapidly fragment.[38]

A critical tool to dissecting the effects of axotomy on the proximal axon, distal axon, and cell body has been the *Wld*^{S} mouse. Wallerian degeneration is slowed in the *Wld*^{S} mouse,[39] and distal neurites remain viable even when the cell body undergoes apoptosis.[40,41] In the optic nerve, both Wallerian degeneration and RGC death after axotomy are slowed.[42] The molecular basis for *Wld*^{S} is an autosomal dominant 85 kb tandem triplication mutation on chromosome 4. This mutation contains nicotinamide mononucleotide adenylyltransferase (NMNAT)-1, an 18 amino acid linkage, and ubiquitination factor E4B. *Wld*^{S} likely induces delivery of NMNAT-1 to the axon and prevents its degeneration after axotomy.[43] The mechanism likely reflects substitution for lack of NMNAT, probably NMNAT-2. Axotomy or other axonal injuries deplete NMNAT-2 from the axon, and cause distal axonal degeneration.[44] Increasing axonal NMNAT-1 levels in the face of decreased NMNAT-2 will therefore mediate increased axonal survival.[43,44] This model would imply that *Wld*^{S} should improve both proximal and distal axotomy after survival.

However, in the dopaminergic nigrostriatal pathway, the *Wld*^{S} genotype protects against Wallerian, but not retrograde axonal degeneration.[45] This implies that there are mechanisms for retrograde axonal degeneration that are fundamentally different from Wallerian degeneration, although a role for gradients in axonal transport of *Wld*^{S} cannot be excluded.[43] One such mechanism was suggested by the ability of constitutively active myristoylated Akt to protect retrograde degeneration of dopaminergic nigrostriatal axons in axotomy and neurotoxin models.[46] Conversely, absence of translation elongation factor eEF1A2 (*Wasted*) delays Wallerian but not retrograde degeneration in the motor system.[47]

Nonetheless, the present results support a similar time course and magnitude of retrograde and Wallerian degeneration after axotomy of unmyelinated axons within the central nervous system, as demonstrated by noninvasive real-time optical imaging techniques in living animals. Although these two types of axonal degeneration can differ under specific circumstances, it is possible that they also share critical pathophysiological mechanisms. Understanding those mechanisms could lead to better techniques for preventing axonal degeneration in the nervous system.

References

1. Raff MC, Whitmore AV, Finn JT: Axonal self-destruction and neurodegeneration. Science 2002, 296:868–871
2. Coleman MP, Freeman MR: Wallerian degeneration. Wld(S), and Nmnat. Annu Rev Neurosci 2010, 33:245–267
3. Kerschensteiner M, Schwab ME, Lichtman JW, Misgeld T: In vivo imaging of axonal degeneration and regeneration in the injured spinal cord. Nat Med 2005, 11:572–577
4. Knoferle J, Koch JC, Ostendorf T, Michel U, Planchamp V, Vutova P, Tonges L, Stadelmann C, Bruck W, Bahr M, Lingor P: Mechanisms of acute axonal degeneration in the optic nerve in vivo. Proc Natl Acad Sci USA 2010, 107:6064–6069
5. Vincent P, Maskos U, Charvet I, Bourgeais L, Stoppini L, Leresche N, Changeux JP, Lambert R, Meda P, Paupardin-Tritsch D: Live imaging of neural structure and function by fibred fluorescence microscopy. EMBO Rep 2006, 7:1154–1161
6. Svoboda K, Yasuda R: Principles of two-photon excitation microscopy and its applications to neuroscience. Neuron 2006, 50:823–839
7. Misgeld T, Kerschensteiner M, Bareyre FM, Burgess RW, Lichtman JW: Imaging axonal transport of mitochondria in vivo. Nat Methods 2007, 4:559–561
8. Wang X, Schwarz TL: Imaging axonal transport of mitochondria. Methods Enzymol 2009, 457:319–333
9. Ey B, Kobsar I, Blazyca H, Kroner A, Martini R: Visualization of degenerating axons in a dysmyelinating mouse mutant with axonal loss. Mol Cell Neurosci 2007, 35:153–160
10. Cordeiro MF, Guo L, Luong V, Harding G, Wang W, Jones HE, Moss SE, Sillito AM, Fitzke FW: Real-time imaging of single nerve cell apoptosis in retinal neurodegeneration, Proc Natl Acad Sci USA 2004, 101:13352–13356
11. Schmitz-Valckenberg S, Guo L, Maass A, Cheung W, Vugler A, Moss SE, Munro PM, Fitzke FW, Cordeiro MF: Real-time in vivo imaging of

retinal cell apoptosis after laser exposure. Invest Ophthalmol Vis Sci 2008, 49:2773–2780
12. Kanamori A, Catrinescu MM, Kanamori N, Mears KA, Beaubien R, Levin LA: Superoxide is an associated signal for apoptosis in axonal injury. Brain 2010, 133:2612–2625
13. Kanamori A, Catrinescu MM, Traistaru M, Beaubien R, Levin LA: In vivo imaging of retinal ganglion cell axons within the nerve fiber layer. Invest Ophthalmol Vis Sci 2010, 51:2011–2018
14. Selles-Navarro I, Ellezam B, Fajardo R, Latour M, McKerracher L: Retinal ganglion cell and nonneuronal cell responses to a microcrush lesion of adult rat optic nerve. Exp Neurol 2001, 167:282–289
15. Comley LH, Wishart TM, Baxter B, Murray LM, Nimmo A, Thomson D, Parson SH, Gillingwater TH: Induction of cell stress in neurons from transgenic mice expressing yellow fluorescent protein: implications for neurodegeneration research. PLoS One 2011, 6:e17639
16. Kim YE, Chen J, Langen R, Chan JR: Monitoring apoptosis and neuronal degeneration by real-time detection of phosphatidylserine externalization using a polarity-sensitive indicator of viability and apoptosis. Nat Protoc 2010, 5:1396–1405
17. Kim YE, Chen J, Chan JR, Langen R: Engineering a polarity-sensitive biosensor for time-lapse imaging of apoptotic processes and degeneration. Nat Methods 2010, 7:67–73
18. Berkowitz BA, Lukaszew RA, Mullins CM, Penn JS: Impaired hyaloidal circulation function and uncoordinated ocular growth patterns in experimental retinopathy of prematurity. Invest Ophthalmol Vis Sci 1998, 39:391–396
19. Maass A, von Leithner PL, Luong V, Guo L, Salt TE, Fitzke FW, Cordeiro MF: Assessment of rat and mouse RGC apoptosis imaging in vivo with different scanning laser ophthalmoscopes. Curr Eye Res 2007, 32:851–861
20. Mansour-Robaey S, Clarke DB, Wang YC, Bray GM, Aguayo AJ: Effects of ocular injury and administration of brain-derived neurotrophic factor on survival and regrowth of axotomized retinal ganglion cells, Proc Natl Acad Sci USA 1994, 91:1632–1636
21. Inoue T, Hosokawa M, Morigiwa K, Ohashi Y, Fukuda Y: Bcl-2 overexpression does not enhance in vivo axonal regeneration of retinal ganglion cells after peripheral nerve transplantation in adult mice. J Neurosci 2002, 22:4468–4477
22. Brown A: Slow axonal transport: stop and go traffic in the axon. Nat Rev Mol Cell Biol 2000, 1:153–156
23. Coleman MP, Perry VH: Axon pathology in neurological disease: a neglected therapeutic target. Trends Neurosci 2002, 25:532–537
24. Toffoli D, Levin LA: Optic nerve axonal injury. Ocular Disease: Mechanisms and Management. Edited by Levin LA, Albert DM. New York, Elsevier, 2010, pp 322–329.
25. Kawaguchi I, Higashide T, Ohkubo S, Takeda H, Sugiyama K: In vivo imaging and quantitative evaluation of the rat retinal nerve fiber layer using scanning laser ophthalmoscopy. Invest Ophthalmol Vis Sci 2006, 47:2911–2916
26. Cengiz N, Ozturk G, Erdogan E, Him A, Elif OK: Consequences of neurite transection in vitro. J Neurotrauma 2010, doi:10.1089/neu.2009.0947
27. Ziv NE, Spira ME: Axotomy induces a transient and localized elevation of the free intracellular calcium concentration to the millimolar range. J Neurophysiol 1995, 74:2625–2637
28. Spira ME, Oren R, Dormann A, Gitler D: Critical calpain-dependent ultrastructural alterations underlie the transformation of an axonal segment into a growth cone after axotomy of cultured Aplysia neurons. J Comp Neurol 2003, 457:293–312
29. Gitler D, Spira ME: Real time imaging of calcium-induced localized proteolytic activity after axotomy and its relation to growth cone formation. Neuron 1998, 20:1123–1135
30. Meiri H, Dormann A, Spira ME: Comparison of ultrastructural changes in proximal and distal segments of transected giant fibers of the cockroach Periplaneta americana. Brain Res 1983, 263:1–14
31. Smith RS, Bisby MA: Persistence of axonal transport in isolated axons of the mouse. Eur J Neurosci 1993, 5:1127–1135
32. Wine JJ: Invertebrate central neurons: orthograde degeneration and retrograde changes after axonotomy. Exp Neurol 1973, 38:157–169
33. Bittner GD: Long Term Survival of Severed Distal Axonal Stumps in Vertebrates and Invertebrates. American Zoologist 1988, 28:1165–1179
34. Erez H, Spira ME: Local self-assembly mechanisms underlie the differential transformation of the proximal and distal cut axonal ends into functional and aberrant growth cones. J Comp Neurol 2008, 507:1019–1030
35. Villegas-Perez MP, Vidal-Sanz M, Bray GM, Aguayo AJ: Influences of peripheral nerve grafts on the survival and regrowth of axotomized retinal ganglion cells in adult rats. J Neurosci 1988, 8:265–280
36. Giftochristos N, David S: Laminin and heparan sulphate proteoglycan in the lesioned adult mammalian central nervous system and their possible relationship to axonal sprouting. J Neurocytol 1988, 17:385–397
37. Conforti L, Adalbert R, Coleman MP: Neuronal death: where does the end begin? Trends Neurosci 2007, 30:159–166
38. Beirowski B, Berek L, Adalbert R, Wagner D, Grumme DS, Addicks K, Ribchester RR, Coleman MP: Quantitative and qualitative analysis of Wallerian degeneration using restricted axonal labelling in YFP-H mice. J Neurosci Methods 2004, 134:23–35
39. Lunn ER, Perry VH, Brown MC, Rosen H, Gordon S: Absence of Wallerian degeneration does not hinder regeneration in peripheral nerve. Eur J Neurosci 1989, 1:27–33
40. Deckwerth TL, Johnson EM, Jr.: Neurites can remain viable after destruction of the neuronal soma by programmed cell death (apoptosis). Dev Biol 1994, 165:63–72
41. Beirowski B, Babetto E, Coleman MP, Martin KR: The WldS gene delays axonal but not somatic degeneration in a rat glaucoma model. Eur J Neurosci 2008, 28:1166–1179
42. Perry VH, Brown MC, Lunn ER: Very slow retrograde and wallerian degeneration in the CNS of C57BL/Ola mice. Eur J Neurosci 1991, 3:102–105
43. Babetto E, Beirowski B, Janeckova L, Brown R, Gilley J, Thomson D, Ribchester RR, Coleman MP: Targeting NMNAT1 to axons and synapses transforms its neuroprotective potency in vivo. J Neurosci 2010, 30:13291–13304
44. Gilley J, Coleman MP: Endogenous Nmnat2 is an essential survival factor for maintenance of healthy axons. PLoS Biol 2010, 8:e1000300
45. Cheng HC, Burke RE: The WldS mutation delays anterograde, but not retrograde, axonal degeneration of the dopaminergic nigro-striatal pathway in vivo. J Neurochem 2010, 113:683–691
46. Cheng HC, Kim SR, Oo TF, Kareva T, Yarygina O, Rzhetskaya M, Wang C, During M, Talloczy Z, Tanaka K, Komatsu M, Kobayashi K, Okano H, Kholodilov N, Burke RE: Akt suppresses retrograde degeneration of dopaminergic axons by inhibition of macroautophagy. J Neurosci 2011, 31:2125–2135
47. Murray LM, Thomson D, Conklin A, Wishart TM, Gillingwater TH: Loss of translation elongation factor (eEF1A2) expression in vivo differentiates between Wallerian degeneration and dying-back neuronal pathology. J Anat 2008, 213:633–645